Environmental Science and Pollution Research (2018) 25:23817–23832
https://doi.org/10.1007/s11356-018-2391-6

RESEARCH ARTICLE

Removal of two anionic reactive textile dyes by adsorption into MgAl-layered double hydroxide in aqueous solutions

Saber Boubakri[1,2] · Mohamed Amine Djebbi[3,4,5] · Zaineb Bouaziz[3,6] · Philippe Namour[5] · Nicole Jaffrezic-Renault[4] · Abdesslem Ben Haj Amara[3] · Malika Trabelsi-Ayadi[1] · Ibtissem Ghorbel-Abid[2] · Rafik Kalfat[2]

Received: 31 October 2017 / Accepted: 23 May 2018 / Published online: 6 June 2018

Abstract

Textile dyes pose a significant challenge for water pollution due to the poor degradability of their complex aromatic structures (e.g., RR-120 and RBB-150). In order to minimize the harmful effects of RR-120 and RBB-150, the capacity of MgAl-layered double hydroxide for removing of these contaminants was studied herein. Batch adsorption experiments were conducted to investigate the effect of various operating parameters, such as solution pH, contact time, dye concentration, and temperature in order to provide optimal conditions for removal. Structural and morphological analyses were used to highlight the assembly and/or interaction LDH-dye. The state of equilibrium of RR-120 and RBB-150 adsorption was pH- and temperature-dependent and followed the pseudo-second-order rate model. Also, the equilibrium adsorption data of both dyes were found to adopt the Langmuir type isotherm model, which assumes a monolayer arrangement in LDH-dye. Furthermore, the effects of four major coexisting and competing mono- and divalent interlayer anions, such as NO_3^-, Cl^-, CO_3^{2-}, and SO_4^{2-}, on the uptakes of RR-120 and RBB-150 were studied and the results showed that NO_3^- anions had insignificant effect on the uptakes of RR-120 and RBB-150 by MgAl. An equivalent study on the presence of both dyes in competitive trial adsorption/desorption from binary aqueous solution was investigated. And finally, the reuse operation of recovered material after dye adsorption was tested in up to 5 cycles of recyclability.

Keywords Reactive Red-120 (RR-120) · Reactive Blue Bezaktiv-150 (RBB-150) · Layered double hydroxide (LDH) · Hydrotalcite (HT) · Adsorption/desorption · Remediation · Reusability

Responsible editor: Philippe Garrigues

✉ Mohamed Amine Djebbi
mohammed-amine.djebbi@irstea.fr; med-djebbi@hotmail.fr

[1] Laboratoire des Applications de la Chimie aux Ressources et Substances Naturelles et à l'Environnement, Université de Carthage, Faculté des Sciences de Bizerte, 7021 Zarzouna, Tunisia

[2] Laboratoire Matériaux, Traitement et Analyse, BiotechPole Sidi-Thabet, Institut National de Recherche et d'Analyse Physico-chimique, 2020 Ariana, Tunisia

[3] Laboratoire de Physique des Matériaux Lamellaires et Nanomatériaux Hybrides, Université de Carthage, Faculté des Sciences de Bizerte, 7021 Zarzouna, Tunisia

[4] Institut des Sciences Analytiques UMR CNRS 5280, Université de Lyon, 5 rue de la Doua, 69100 Villeurbanne, France

[5] UR RiverLy, Centre de Lyon-Villeurbanne, Irstea, 5 rue de la Doua CS 20244, 69625 Villeurbanne, France

[6] Institut Européen des Membranes, UMR5635 UM ENSM CNRS, Place Eugène Bataillon, 34095 Montpellier cedex 5, France

Introduction

Clean water is a finite and vulnerable resource essential for all living organisms to sustain life, development, and environment. Preventing contamination and minimizing waste become a serious question worrying the society. However, the growing demand for new and more diverse products and technological developments influences our society and spurs the rising use of synthetic chemicals, which in turn increases the emission of pollutants and by-products harmful to human health and ecosystem.

Over a large range, synthetic dyes resulting from the industrial use, including textiles, leather, dyeing, paints, and printing, in food and pharmaceutical or cosmetic applications, and in metallurgy process, plastics, and agro-chemistry are one of the most pollutants releasing industries of the world (El Hassani et al. 2017; Santos et al. 2017). They are continuously causing unimaginable harm to the environment. Indeed, the presence of these substances in aquatic environment reduces

light penetration and disturbs biological cycles of aquatic biota, potentially affecting the photochemical activities (McMullan et al. 2001; Robinson et al. 2002; Pereira and Freire 2005). Moreover, the presence of these toxic pollutants in drinking water may cause severe damage to human beings, such as renal dysfunction, reproductive system, liver, brain, and central nervous system, and have been characterized as mutagenic and carcinogenic (Özcan and Özcan 2004; Abdellaoui et al. 2017; Mahjoubi et al. 2017). Particularly, reactive dyes represent the major category of the synthetic dyes. They are extensively used in textile industries, due to their excellent binding ability with textile fibers through covalent bonds between reactive group and fiber (Darsana et al. 2015).

Reactive Red-120 (RR-120) and Reactive Blue Bezaktiv-150 (RBB-150) are one of the oldest synthetic dyes that are frequently employed in many industrial sectors especially in dyeing clothes. However, dyeing processes based on the use of reactive dyes generate a massive amount of unfixed dyes and the wastewater as by-product of this process may interfere with the ecosystem through the effluent discharges. Surveys show that nearly 20% of total global production is lost during dyeing process and disposed in wastewater (Hossein and Behzad 2012). Consequently, by virtue of poor degradability and the detrimental effect on the environment, parallel to the substantial amount discharged into wastewater, various methods of removing and degrading these compounds have been studied taking into account the rational and efficiency factors. Among them, membrane filtration, biological treatment, adsorption, electrochemical and photochemical methods, coagulation/flocculation, degradation, and ozonation (Dos Santos et al. 2007; Singh and Arora 2011).

Despite the above-mentioned water treatment methods, most of them are highly operation and maintenance costs. Of all these methods, adsorption process has wide industrial applicability/utility and has been proved to be an effective and economically feasible technique to treat colored effluents, since it combines low-cost, simple operation, availability of different adsorbent, and high removal rate (Santhosh et al. 2016). However, the tangible drawback of this method is the high-cost and tedious procedure for the regeneration of the conventional sorbent (i.e., activated carbon); hence, the need for a cheaper and equally effective substitutes is still required to meet this difficult task. Attention has been focused on the development of the substitutes occurring from natural clay materials.

Synthetic hydrotalcite-like materials (HT), such as layered double hydroxide (LDH), have received extensive attention over the last decade in the removal of various contaminant species from aqueous solutions (Forano 2004; Rojas 2012, Zubair et al. 2017). Also defined as anionic clay, LDH consists of brucite-like layers in which a part of divalent cations are substituted by trivalent cations. The general LDH formula can be expressed as $[M^{II}_{1-x}M^{III}_{x}(OH)_2]^{x+}[A^{n-}_{x/n}{\cdot}yH_2O]$ (abbreviated as $M^{II}M^{III}$-A, where M^{II} is a divalent metal cation, such as Mg^{2+}, Mn^{2+}, Ni^{2+}, Zn^{2+}, Co^{2+}, Fe^{2+}, and Cu^{2+}, and M^{III} is a trivalent metal cation, such as Al^{3+}, Fe^{3+}, Co^{3+}, Ni^{3+}, Mn^{3+}, and Cr^{3+}). The metal cations occupy the octahedral interstices of brucite-like layers and giving rise to excessive positive charge on the surface of sheets, while A^{n-} represents the intercalated anions ensuring the neutrality of the lamellar edifice (Fig. 1) (Djebbi et al. 2016). LDH materials exhibit attractive structural properties favorable for the adsorption of pollutants such as dyes, which is exciting for an environmental scientist. They have specific features like low-cost, easy handling, high surface area, appropriate porosity, lamellar architecture (Gu et al. 2015), no toxic, unhazardous (Carretero 2002; Delhoyo 2007), anion exchange property (Liang et al. 2013), and good thermal stability (Mahjoubi et al. 2017). Thus, LDH is a perfect candidate that would offer a prospect for eco-friendly and environmentally benign technologies of remediation.

In this optic, attempt was made to evaluate the removal ability of MgAl LDH toward two anionic reactive dyes, RR-120 and RBB-150, from aqueous solution in batch adsorption experiments. The physicochemical features of the samples were characterized by powder XRD, FTIR, SEM, TEM, and BET. Factors restricting sorption performance, such as solution pH, time, dye concentration, and temperature, were

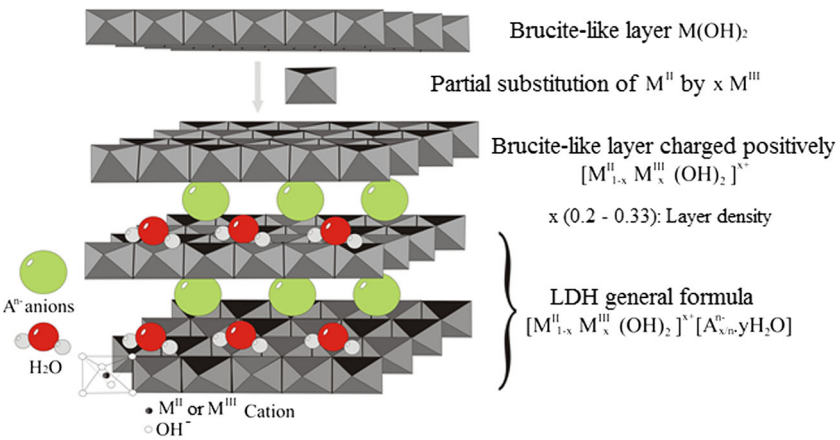

Fig. 1 Schematic representation of the crystal structure of the layered double hydroxide

investigated. The dye uptake and recovery mechanisms supported by kinetic laws and isotherm models were also discussed. Additionally, the competitive adsorption/desorption of RR-120 and RBB-150 from binary system was carried out to better understand the fixation and remobilization of dye compounds in multi-dye contaminated environments. This work devotes also to recover the adsorbent after adsorption in order to ascertain the feasibility of recycling operations.

Materials and methods

Materials and reagents

Reactive Red-120 and Reactive Blue Bezaktiv-150 (Fig. 2, Table 1) were provided by a cotton dyeing company located in Bizerte, Tunisia. The dyes were used as received. Dye stock solutions were prepared by dissolving an appropriate amount of dye (1 g/L) in deionized water and subsequently diluting to required concentrations. Aluminum chloride hexahydrate (99%, CAS 7784-13-6), hydrochloric acid (37%, CAS 7647-01-0), magnesium chloride hexahydrate (98%, CAS 7791-400-6), sodium carbonate (≥ 99%, CAS 497-19-8), sodium chloride (≥ 99%, CAS 7647-14-5), sodium hydroxide (97%, CAS 1310-73-2), sodium nitrate ((≥ 99%, CAS 7631-99-4), and sodium sulfate (≥ 99%, CAS 7757-82-6) were analytical grade, purchased from Prolabo, and used without any further purification.

Synthesis of MgAl-NO_3-layered double hydroxide

The adsorbent MgAl LDH intercalated with NO_3^- was prepared using the co-precipitation method at room temperature

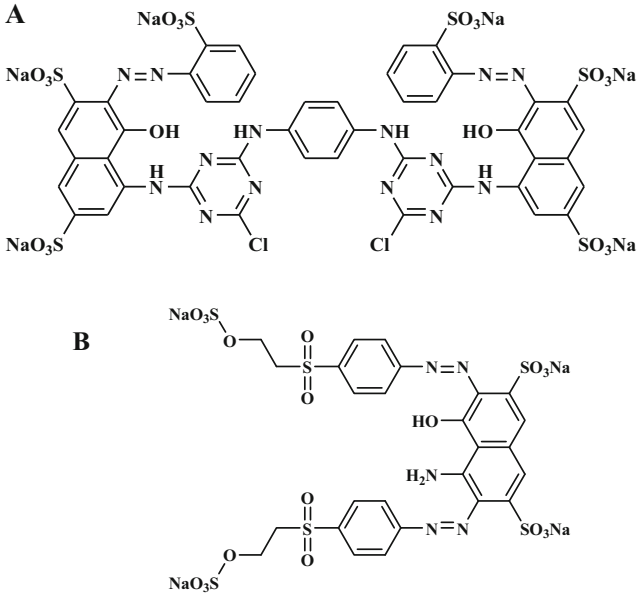

Fig. 2 Molecular structure of **a** RR-120 and **b** RBB-150

Table 1 Physicochemical properties of used dyes

Dye name	Reactive Red-120 (RR-120)	Reactive Blue Bezaktiv-150 (RBB-150)
Chemical formula	$C_{44}H_{24}Cl_2N_{14}Na_6O_{20}S_6$	$C_{26}H_{21}N_5Na_4O_{19}S_6$
Nature	Anionic diazo	Anionic diazo
Molecular weight (g/mol)	1469.98	960
λ_{max} (nm)	535	620

as follows (Djebbi et al. 2016): an aqueous solution (50 mL) containing 33.0 mmol of $MgCl_2{\cdot}6H_2O$ and 16.5 mmol of $AlCl_3{\cdot}6H_2O$ with a molar ratio Mg^{2+}:Al^{3+} of 2 was added dropwise to a solution of 0.5-M $NaNO_3$ (100 mL) under vigorous stirring and nitrogen gas flow. The mixture was maintained at pH 9.0 by adding 2 M of aqueous NaOH solution with a constant flow of 0.12 mL/min using a syringe-pump system (Razel) equipped with a pH meter (αlpha-pH1000 Eutech Instruments), which allows the pH to be maintained constant. The suspension was aged for 24 h under stirring and nitrogen gas flow. The resulting gel was then separated by centrifugation, washed thoroughly with deionized water several times until no Cl^- ions are present, and finally dried and kept at room temperature for 24 h.

Batch adsorption experiments

Determination of the diazo dye concentrations

The concentrations of RR-120 and RBB-150 in the supernatant are determined eventually from the standard curve obtained using an UV-Vis spectrophotometer (T60UV-Visible spectrophotometer) by measuring the absorbance at 535 and 620 nm, respectively, in a quartz cuvette with 10-mm path length.

Initial pH effect on dye removal

To study the effect of pH on the adsorption of RR-120 and RBB-150 dyes onto MgAl-NO_3 LDH, the suspension pH was prepared by adding 50 mg of LDH to 100 mL of dye solutions (200 mg/L). The tested initial pH values were adjusted in the range 3.0–12.0 by adding 0.1-M HCl or 0.1-M NaOH. The final pH was measured at the end of the experiments.

All experiments were performed in triplicate.

Adsorption kinetics

Kinetic experiments were conducted on the dynamic of dye uptake onto LDH and on the quantification of the adsorption rate. The kinetics of RR-120 and RBB-150 retention by MgAl-NO_3 LDH was investigated at 25 °C in a thermostatic bath under stirring for different times (0–120 min). Typically,

50 mg of the LDH was added to 100 mL of dye solutions (200 mg/L). At pre-set time intervals, suspensions were separated through centrifugation and examined spectrophotometrically in order to estimate the amount of dye adsorbed at time t, q_t (mg/g) Eq. (1).

$$q_t = (C_0 - C_t)\frac{V}{m} \quad (1)$$

where C_0 and C_t are the initial concentration and the concentration at specified time t of dye, respectively, V (L) is the volume of the dye solution, and m (g) is the mass of the adsorbent.

All experiments were performed in triplicate.

Adsorption isotherms and thermodynamic study

Adsorption isotherms were performed using the batch equilibrium method by plotting the amount of adsorbed dye q_e (mg/g) vs. the equilibrium concentration in the solution C_e (mg/L). Typically, 50 mg of LDH was dispersed into a series of 200-mL flask containing 100 mL of diluted dye solutions ranged from 10 to 500 mg/L. The suspension flasks were stirred and kept in a thermostatic bath at 25, 30, 35, and 40 °C. Afterwards, the suspensions were separated through centrifugation and analyzed by UV-Vis spectrophotometry, and the percentage of the dye removal and the amount of dye adsorbed at equilibrium q_e were calculated using the following equations:

$$q_e = (C_0 - C_e)\frac{V}{m} \quad (2)$$

$$\text{Dye removal}\ (\%) = 100\frac{C_0 - C_e}{C_0} \quad (3)$$

where C_0 and C_e are the initial concentration and the equilibrium concentration of dye, respectively, V (L) is the volume of the dye solution, and m (g) is the mass of the adsorbent.

All experiments were performed in triplicate.

Competing effect of interlayer anion

Single-point batch experiments of RR-120 and RBB-150 dye solutions containing different competing inorganic anions (i.e., NO_3^-, Cl^-, CO_3^{2-}, and SO_4^{2-}) were prepared by dissolving various amount of their sodium salts along 100 mL of diluted dye solutions (500 mg/L) in different concentrations ratios (1/4, 1/2, 1/1, 3/2, and 2/1). Fifty-milligram LDH then was added to each of the solutions on a shaker. The solid and solution phases were separated by centrifugation, and supernatant solution was collected for dye analysis.

All experiment was performed in triplicate.

Competitive adsorption/desorption

For competitive experiments, the same adsorption experiment conditions were followed; 50 mg of LDH was dispersed into 100 ml of mixed dye solution (the initial dye concentration was fixed at 500 mg/L, and the mass ratio of RR-120 and RBB-150 was 1:1) at pH 5 and for contact time of 120 min (25 °C). The desorption efficiency is determined by injecting a known amount of dye onto the sorbent with 100 mL of deionized water for 24 h, desorbing it, and analyzing the amount recovered, referring to the following equation:

$$\text{Desorption}\ (\%) = 100\ \frac{\text{Released dye}}{\text{Retained dye}} \quad (4)$$

All experiments were performed in triplicate.

Adsorbent reusability

The reusability of the adsorbent was evaluated by repeated adsorption-calcination-rehydration cycles. An amount of 50 mg of LDH was dispersed into 100-mL dye solutions (500 mg/L) and stirred for 120 min at 25 °C. After the adsorption, the adsorbent was submitted to calcination process at 500 °C for 4 h in order to obtain magnesium-aluminum-layered double oxide MgAl LDO and then the calcined product was rehydrated into the same volume of the dye solutions (200 mg/L) for further reconstruction. This procedure was repeated three times and the residual concentration of dye was determined as above.

Characterizations

X-ray diffractograms were recorded with a conventional θ–θ Bragg–Brentano configuration (Ni-filtered CuK$\alpha_{1,2}$ = 1.5406 Å, at 20 mA, 40 kV) using a model D8 Advance Bruker-AXS Powder X-ray diffractometer coupled with a linear Vantec-1 detector. The diffraction patterns were performed between 2 and 70° (2θ) with angular and time steps of 0.0330° and 1,006,952 s, respectively.

Fourier-transform infrared spectra (FTIR) in absorbance mode were recorded using a Nicolet 200 FTIR (Thermo Scientific) spectrophotometer in the range of 4000–400 cm^{-1}. The spectra were recorded during 64 scans and with a resolution scan of 1 cm^{-1}.

Quantitative determinations of loaded and released dyes were acquired using T60UV-Visible spectrophotometer with scanning rate of 1 nm s^{-1}.

Scanning electron micrographs (SEM) were recorded on a Jeol JSM-5400 and Hitachi S-4800 microscopes working at electron energies of 15 and 10 kV, respectively.

Transmission electron nanographs (TEM) were performed on a FEI Tecnai G2 microscope with an accelerating voltage of 200 kV.

Surface area analysis was determined by N_2 adsorption/desorption at 200 °C on an ASAP 2020 surface area analyzer (Micromeritics Instrument Corporation, USA).

Results and discussions

Physico-chemical characterizations of the sorbent

The MgAl-NO_3 LDH pattern exhibits characteristic reflections typical of hydrotalcite-like compounds (Fig. 3), with intense, symmetric *00l* and *11l* reflection lines and less intense, asymmetric *01l* lines and can be indexed in a hexagonal lattice with an $R\bar{3}$ m rhombohedral space group symmetry (Chitrakar et al. 2008; Feng et al. 2012). The intense reflection lines *003* and *006* at low 2θ angles (11.44°–23.09°), whose positions depend on the size of the intercalated anion provide an information on the basal spacing and allow to calculate the lattice parameter c ($c = \frac{3}{2}[d_{003} + 2d_{006}]$), while the reflection line *110* at high 2θ (62.19°) provides an information on the average cation-cation distance and allows to calculate the lattice parameter a ($a = 2d_{110}$) (Perez-Ramírez et al. 2001). Determined parameters c and a are shown in Table 2. The values of the basal spacing d_{003} and d_{110} are in the order of 0.872 and 0.152 nm, respectively (Table 2), corresponding to hydrotalcite with nitrate as interlayer anion and a molar ratio Mg^{2+}:Al^{3+} of 2 (Evans and Slade 2006). The crystallite size calculated by a Scherrer calculator using PANalytical X'Pert HighScore Plus software from the full-width at half-maximum (FWHM) intensity of the *003* reflection is estimated to be roughly 112.5 nm, revealing in a higher surface area of 159 m^2/g and higher exchange capacity of 360 mEq/100 g (Table 2).

Table 2 Crystallographic data of MgAl-NO_3 LDH, specific surface area (m^2/g), and anionic exchange capacity (mEq/100 g)

LDH	d_{003} (nm)	d_{110} (nm)	Crystallite size D (nm)	Lattice parameters		S_{BET} (m^2/g)	A.E.C. (mEq/100 g)
				c (nm)	a (nm)		
MgAl-NO_3	0.872	0.152	112.5	2.616	0.304	159	360

The FTIR spectra included in Fig. 4 revealed the characteristic bonds corresponding to hydrotalcite-like structure. The broad and strong band centered at 3491 cm^{-1} is attributed to the stretching modes of hydroxyl groups derived from both brucitic sheets and water molecules located into the interlayer space and on the external surface of the sheets. A standard area is observed in the range 2750–1750 cm^{-1}, corresponding to the background noise. The bands recorded at the medium region correspond to the bending mode of water molecules (1650 cm^{-1}) and the vibration mode of the NO_3^- interlayer anions (1382 cm^{-1}). Finally, the bands in the region bellow 1000 cm^{-1}, which are assigned to the intrinsic vibrations of tetrahedral and octahedral sites M—O (599 and 839 cm^{-1}) and O—M—O (423 cm^{-1}) inside the brucitic sheets (Rives 2001).

The morphology and the nanostructure of the MgAl-NO_3 LDH sample were investigated using scanning and transmission electron microscopy, respectively, and are illustrated in Fig. 5. As shown, the MgAl-NO_3 sample consists of nanosphere platelets of dimensions ranging between 50 and 200 nm (panels c and d), agglomerated in "sand rose" form, which is the typical structure of the hydrotalcite-like compound (Evans and Duan 2006). Panel e displays the SAED pattern of the LDH nanoparticles, and the observed diffraction rings clearly indicate high crystallinity of the sample and can be indexed to hexagonal polycrystals. These diffraction rings

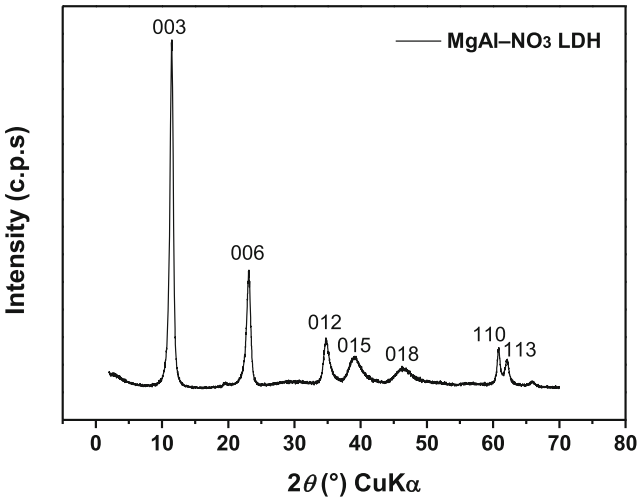

Fig. 3 Powder XRD pattern of MgAl-NO_3 LDH

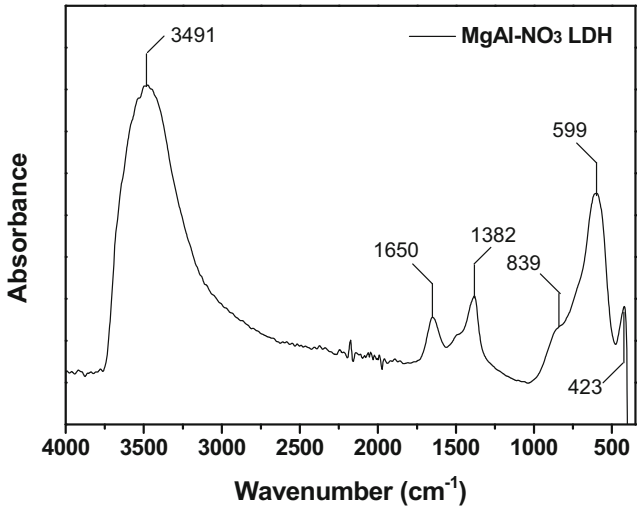

Fig. 4 FT-IR spectra of MgAl-NO_3 LDH

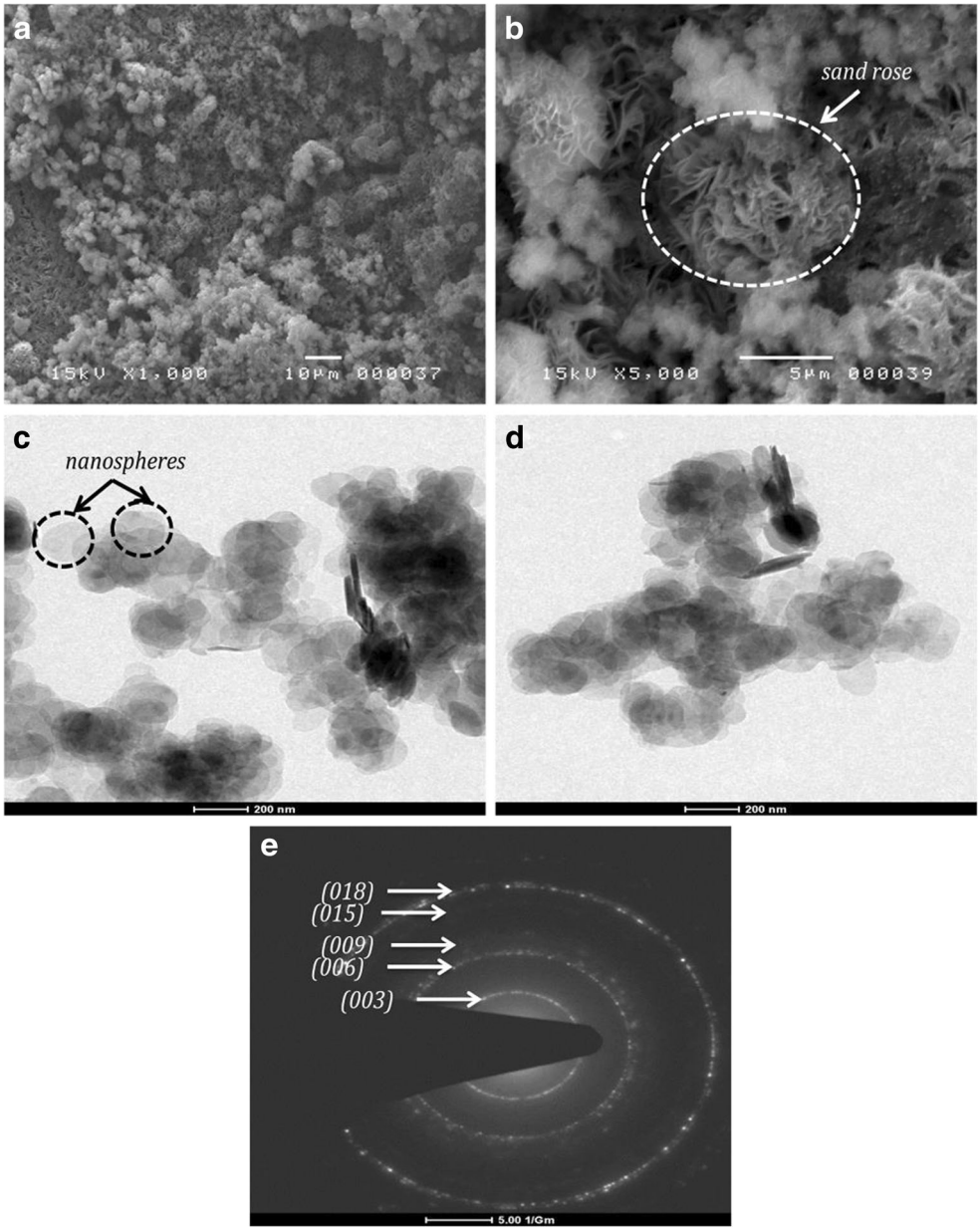

Fig. 5 SEM (**a**, **b**), TEM (**c**, **d**), and SAED (**e**) images of MgAl-NO_3 LDH

were attributed to (*003*), (*006*), (*015*), and (*018*) LDH planes. Thus, the resulted data are in good agreement with those obtained by theoretical computation based on the PXRD measurements.

Adsorption measurements

Effect of initial pH

Initial pH value is one of the important factors controlling the adsorption at water-adsorbent interface. It can affect both the adsorbent binding sites (acting on surface charge of adsorbent by protonation and deprotonation of functional groups) and the chemistry of the dyes in solution (the degree of ionization of dyes) (Ai et al. 2011). In order to evaluate the effect of pH, adsorption experiments were conducted at varying pH (pH 3.0–12.0) with dye solutions of concentration of 200 mg/L and adsorbent dosage of 50 mg for 120 min. Figure 6 shows the variation of the removal efficiency of dyes at different pH values as well as the adsorption capacity q_e. As can be seen from Fig. 6, the adsorption of RR-120 and RBB-150 is obviously dependent on initial solution pH. Maximum adsorption of dyes increased in acidic pH from 3.0 to 5.0 and decreased as the solution pH is above 5.0. Similar results were reported in the literature showing higher uptake in acidic medium (Bazrafshan et al. 2013; Abidi et al. 2014; Naghmouchi and Nahdi 2015). Subsequently, the adsorption experiments were carried out

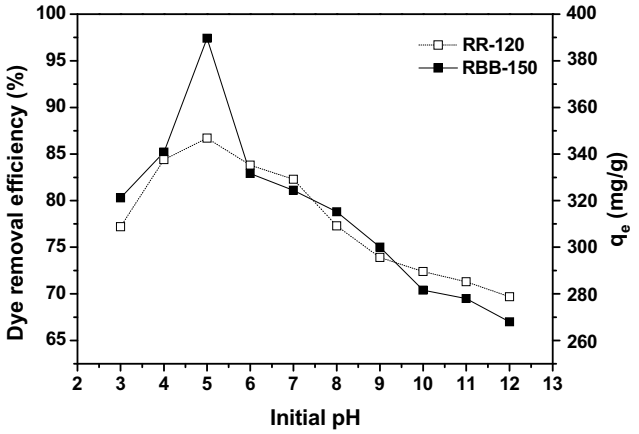

Fig. 6 Effect of initial pH on the adsorption of RR-120 and RBB-150 by MgAl-NO_3 LDH; $C_0 = 200$ mg/L, contact time of 120 min, adsorbent dosage of 50 mg, $T = 25$ °C

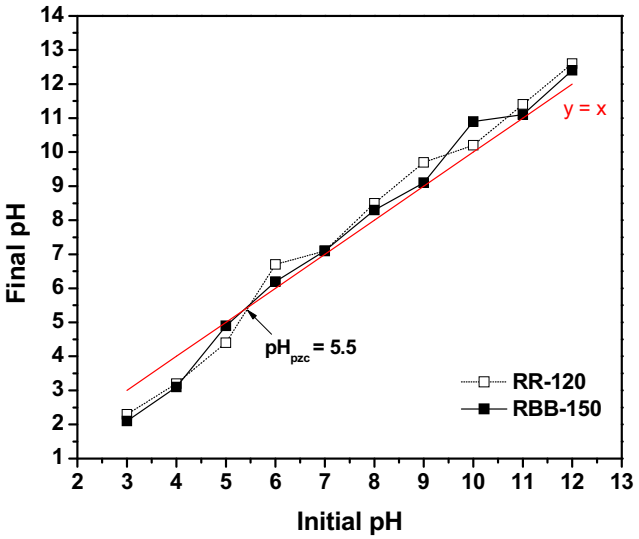

Fig. 7 Plots of final pH against initial pH for the determination of pH_{pzc} of MgAl-NO_3 LDH

at pH of 5.0 in order to reach the optimal adsorption. Indeed, the maximum adsorption capacity of the MgAl-NO_3 LDH at pH 5.0 was 346.8 mg/g, about 86% of removal for RR-120, and 389.6 mg/g when 97% of RBB-150 was removed. Differences in removal rate values may have arose from the affinity of each dye for the LDH. The higher uptake of RBB-150 at pH 5.0 can be explained by the fact that RBB-150 structure contains four benzene rings compared to seven in the structure of RR-120, making it smaller than the latter and favors its access to the positive binding sites of the LDH. Moreover, RBB-150 has pKa values lower than zero (Aguiar et al. 2014), whereas the RR-120 has a pKa value of 4.4 (Errais et al. 2012) and is thus completely ionized at pH 5, with negative charges even in highly acidic solutions due to their sulfonate and sulfato-ethyl-sulfone groups. In this respect, the affinity effect due to having lower pKa is offset by better dissociation and more negative charge making RBB-150 better and preferentially adsorbed than RR-120 at pH 5.0.

However, the low removal at alkaline conditions is due on the one hand to the competition effect between the excess OH^- in the solution and the anionic molecules of RR-120 and RBB-150, and on the other hand, to the electrostatic repulsion between the latter and the negatively charged active adsorption sites on the LDH. The results (Fig. 7) indicated that the pH of the zero point of charge (pH_{pzc}) of MgAl-NO_3 LDH nanoparticles is around 5.5. Let's recall that the surface of LDH consists of hydroxyl groups (═OH); thus, when pH increases above pH_{pzc}, the hydroxyl groups are ionized and the negative charge density on the surface increases. While at lower pH values below pH_{pzc}, the surface of LDH becomes protonated and gets more positively charged, the electrostatic attraction occurs between the positively charged active adsorption sites and the anionic dye molecules, which results in increase of dye removal. This why the maximum adsorption occurred at pH 5.

Kinetics: effect of contact time

The contact time between the pollutants and the adsorbent is one of the most important parameters to control. It gives an insight into the deeper implication of mechanism enabling the removal of pollutants. Figure 8 shows the evolution of the adsorption process of RR-120 and RBB-150 versus time periods ranging from 5 to 120 min on 50 mg of MgAl-NO_3 LDH adsorbent at pH 5.0 and for initial dye concentration of 200 mg/L. The figure indicates that the adsorbed amounts of RR-120 and RBB-150 onto the LDH increased drastically after 60 min of contact time and then continue to increase at a relatively slow speed until a state of equilibrium is reached within 120 min. Naghmouchi and Nahdi (2015) reported similar findings in their study of the adsorption of RR-120 and RBB-150 by Tunisian raw clay. To ensure that the equilibrium state is fully attained, the dye adsorptions must be

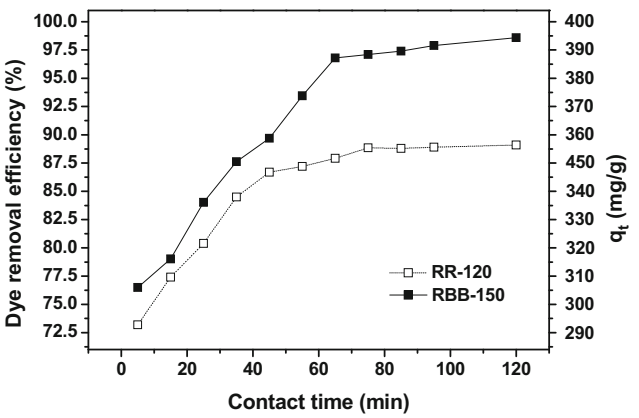

Fig. 8 Effect of contact time on the adsorption of RR-120 and RBB-150 by MgAl-NO_3 LDH; $C_0 = 200$ mg/L, pH = 5, adsorbent dosage of 50 mg, $T = 25$ °C

subsequently performed with a contact time of 120 min. The removal efficiency of RR-120 was found to be about 89% (356.4 mg/g) and that of RBB-150 near 98% (394.4 mg/g). Based on these results, the adsorption phenomenon proceeds in linear progression characterized by a fast rate at the initial stage due to the fact that an abundant number of vacant adsorbent sites are available for adsorption and the higher concentration gradient between the liquid phase and solid-liquid interface. As time proceeds, the access for the remaining vacant surface sites is limited, given the repulsive forces between the dye molecules on the solid and bulk phases, and resulting in a slower rate of adsorption characterized by a "plateau" effect (Bazrafshan et al. 2013; Zhang et al. 2017).

For a deeper understanding on mechanisms involved in the process of adsorption and determining the parameters governing the adsorption kinetics of RR-120 and RBB-150 onto MgAl-NO_3 LDH, the following kinetic models were studied: Lagergren's pseudo-first-order Eq. (5) and pseudo-second-order Eq. (6) (Lagergren 1898; Ho and McKay 1999) and Weber's intra-particle diffusion Eq. (7) (Weber and Morris 1963).

$$\ln(q_e - q_t) = \ln q_e - \left(\frac{k_1}{2.303}\right)t \tag{5}$$

$$\frac{t}{q_t} = \left(\frac{1}{k_2 q_e^2}\right) + \left(\frac{1}{q_e}\right)t \tag{6}$$

$$q_t = k_i t^{0.5} + C \tag{7}$$

where q_e and q_t are the equilibrium adsorption uptake and adsorption uptake at time t, in mg/g, respectively, k_1, k_2, and k_i are the adsorption rate constants of the first- and second-order kinetics and intra-particle diffusion model, in min^{-1}, g mg^{-1} min^{-1}, and mg g^{-1} $min^{-1/2}$, respectively, and C (mg g^{-1}) is the intercept.

Figure 8 shows the straight-line plots of $\ln(q_e - q_t)$ vs. t (Fig. 9a) for the pseudo-first-order, t/q_t vs. t (Fig. 9b) for

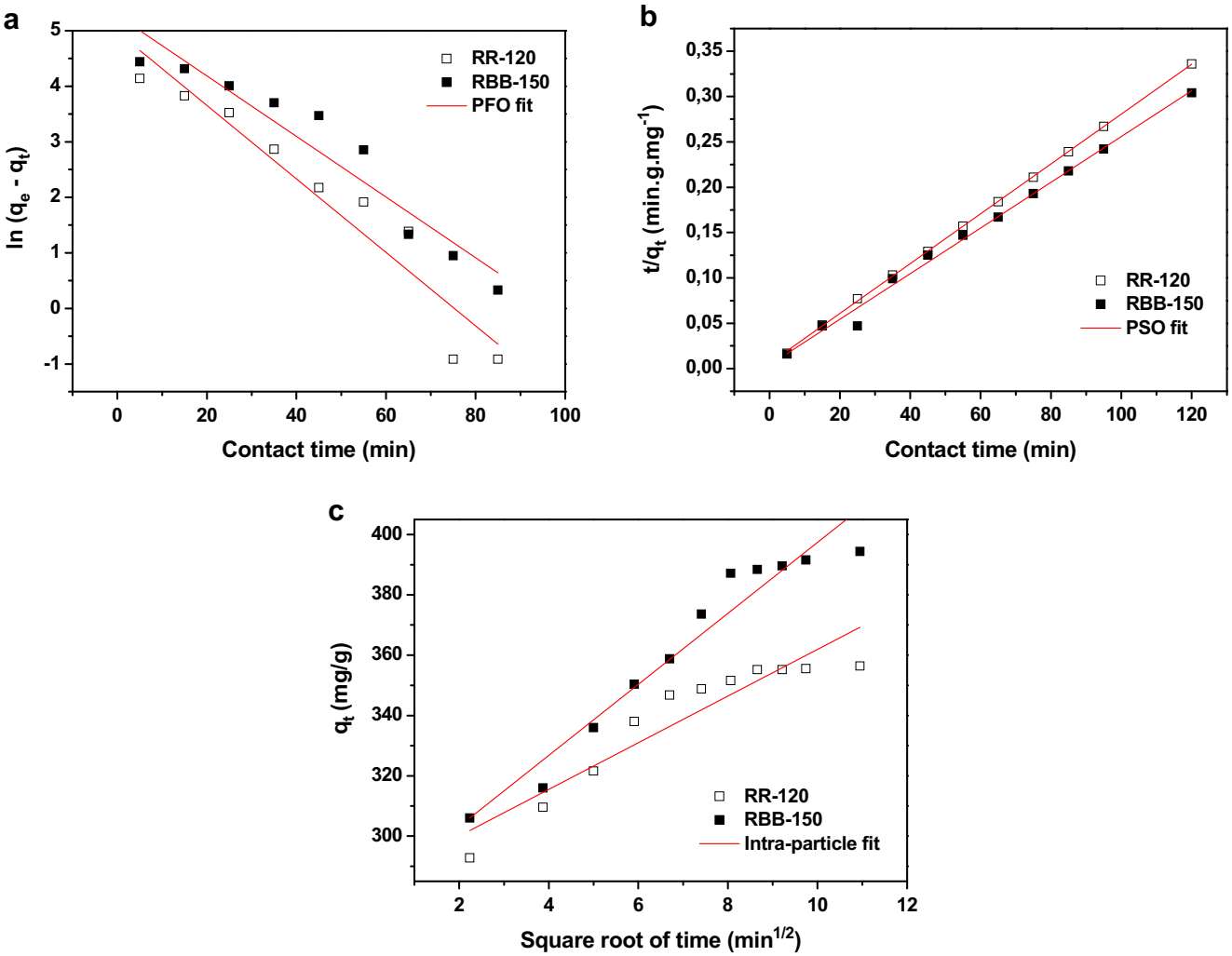

Fig. 9 Kinetic plots for adsorption of RR-120 and RBB-150 on MgAl-NO_3 LDH: **a** pseudo-first-order plot, **b** pseudo-second-order plot, and **c** intra-particle plot

Table 3 Adsorption kinetic parameters of RR-120 and RBB-150 on MgAl-NO_3 LDH

Kinetic model	RR-120	RBB-150
Pseudo-first-order		
$q_{e(exp)}$ (mg/g)	355.6	391.0
$q_{e(cal)}$ (mg/g)	145.0	196.1
k_1(min^{-1})	0.15	0.12
R^2	0.912	0.910
Pseudo-second-order		
$q_{e(exp)}$ (mg/g)	355.6	391.0
$q_{e(cal)}$ (mg/g)	370.3	400.0
k_2 (g mg^{-1} min^{-1})	1.25×10^{-3}	1.60×10^{-3}
R^2	0.999	0.992
Intra-particle diffusion		
$q_{e(exp)}$ (mg/g)	355.6	391.0
C (mg g^{-1})	284.5	279.7
k_i (mg g^{-1} $min^{-1/2}$)	7.73	11.76
R^2	0.871	0.939

pseudo-second order, and q_t against $t^{1/2}$ (Fig. 9c) for intra-particle diffusion model. As seen from the graphic plotting (Fig. 8), the pseudo-first-order and the intra-particle models do not fit well with the full range of times. The calculated values of the kinetic modeling are included in Table 3. According to the table below, the determination coefficient values (R^2) of pseudo-first-order and intra-particle diffusion kinetic models are lower than that of pseudo-second-order, favoring the latter over the formers, and the latter better expressing the sorption of the dyes. Also, the calculated q_e values obtained from the pseudo-second-order agree very well with the experimental data. Nevertheless, these results suggest that the pseudo-second-order adsorption mechanism is predominant and that the overall rate constant of adsorption process appears to be controlled by chemisorption process in conjunction with the chemistry of the LDH and dye molecules. This assumes that the rate of adsorption is proportional to the square rate of the total number of available sites. A similar phenomenon is observed in the adsorption of RR-120 and RBB-150 onto cetylpyridinium-bentonite (Tabak et al. 2010), organophilic clay (Abidi et al. 2014), and Tunisian raw clay (Naghmouchi and Nahdi 2015).

Adsorption isotherms: effect of dye concentration

The initial concentration of dye plays an important role to overcome all mass transfer resistance of dye between the aqueous and solid phase because a certain mass of the solid can absorb only a determined amount of the dye (Anbia and Hariri 2010). The adsorption experiments of RR-120 and RBB-150 were carried out with varying initial dye concentrations in the range of 10–500 mg/L on 50 mg of MgAl-NO_3 LDH adsorbent at pH 5.0 and for contact time of 120 min. The sorption results (Fig. 10) reflect that the adsorption capacity (Fig. 10a) increased gradually with the increase in initial concentration until saturation was reached, while the percent removal (Fig. 10b) decreased upon increasing the dye concentration. Indeed, the maximum adsorption efficiency decreased from 99 to 80% for RR-120 and from 99 to 93% for RBB-150, when the dye concentration increased from 10 to 500 mg/L and the equilibrium adsorption capacity of RR-120 was found to be 800 mg/g and that of RBB-150 at 910 mg/g. These results suggest that the adsorption of RR-120 and RBB-150 dyes onto MgAl-NO_3 LDH is highly dependent on initial concentration of dye. Furthermore, the difference in efficiency rate of adsorption between RR-120 and RBB-150 may be due to the difference in the molecular structure between them. This is in accordance with previous results obtained by Naghmouchi and Nahdi (2015).

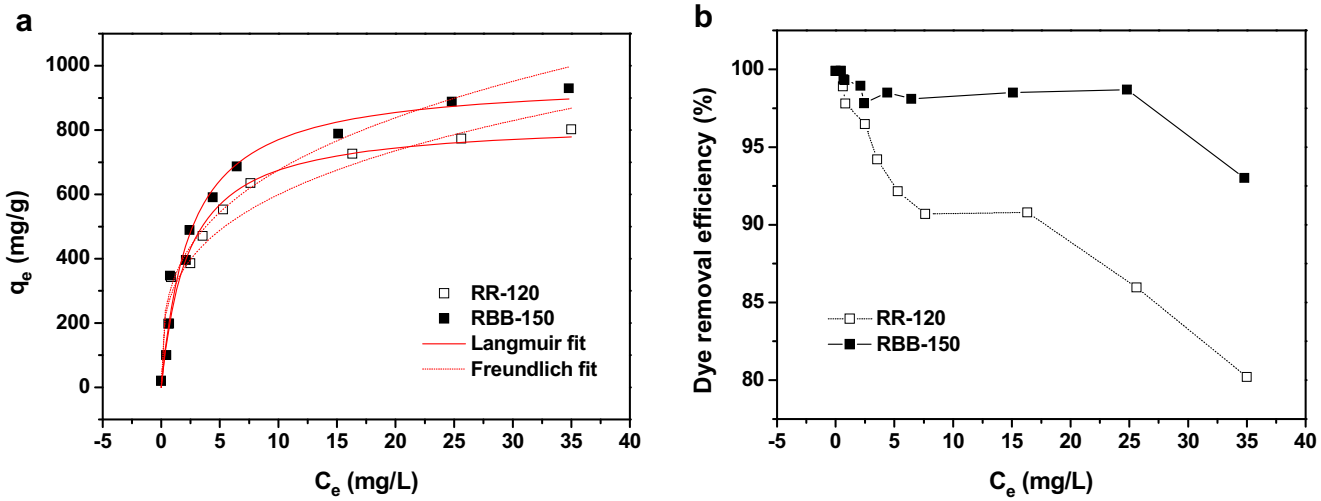

Fig. 10 Effect of dye concentrations on RR-120 and RBB-150 adsorption by MgAl-NO_3 LDH: **a** adsorption capacity and **b** removal percentage; adsorbent dosage of 50 mg, contact time of 120 min, pH = 5, T = 25 °C

Table 4 Langmuir and Freundlich parameters for RR-120 and RBB-150 adsorption onto MgAl-NO_3 LDH

Adsorbent	Dye	$q_{e(exp)}$ (mg/g)	Langmuir isotherm model			Freundlich isotherm model		
			q_{max} (mg/g)	k_L (L/mg)	R^2	K_F	$1/n$	R^2
MgAl-NO_3LDH	RR-120	800	829.9	0.43	0.966	303.4	0.30	0.934
	RBB-150	910	960.5	0.40	0.974	329.6	0.31	0.935

To further understand the interaction of the dye molecules with the adsorbent, the experimental data (Fig. 10a) were analyzed according to the Langmuir Eq. (8) and Freundlich Eq. (9) isotherm models presented below. The models were determined by nonlinear regression analysis.

$$q_e = \frac{q_{max} k_L C_e}{1 + k_L C_e} \quad (8)$$

$$q_e = K_F . C_e^{1/n} \quad (9)$$

where q_{max} (mg/g) is the maximum monolayer adsorption capacity, k_L (L/mg) is the Langmuir constant related to the rate of adsorption, and K_F and n are the Freundlich constants related to adsorption capacity and adsorption intensity, respectively. The calculated parameters of the Langmuir and Freundlich isotherms are listed in Table 4.

Figure 10a displays the typical "L" shape according to Giles's classification (Giles et al. 1974), which suggests a progressive saturation of the sorbent due to the lack in the number of vacant sites. In fact, the large number of active sites of the adsorbent is available at lower initial dye concentrations, resulting in greater adsorbed amount of dye; therefore, adsorption capacity is almost constant at higher concentrations due to non-availability of adsorbent sites for further adsorption. As displayed in Fig. 10a, a possible fit with Freundlich model is observed but Langmuir model fits better. Also, considering the values of the determination coefficients (R^2) and the calculated adsorption capacities (q_{max}) (Table 4), the Langmuir equation gives the best satisfactory fitting to the adsorption equilibrium of RR-120 and RBB-150 onto the LDH sample. The main assumption of this model is that the distribution of active sites on the adsorbent is homogeneous, and each site is likely to fix only one solute molecule (localized adsorption) and no further adsorption can occur at this site. The maximum adsorption capacity corresponds to a saturated monolayer of solute molecules on the adsorbent surface (Langmuir 1918).

To gain more insight into how adsorption mechanism of RR-120 and RBB-150 onto MgAl-NO_3 LDH might be done, the resultant samples after adsorption were recovered and further characterized by PXRD and SEM analyses (Fig. 11).

The PXRD patterns are shown in Fig. 11a. Significant modification is observed compared to the sample before

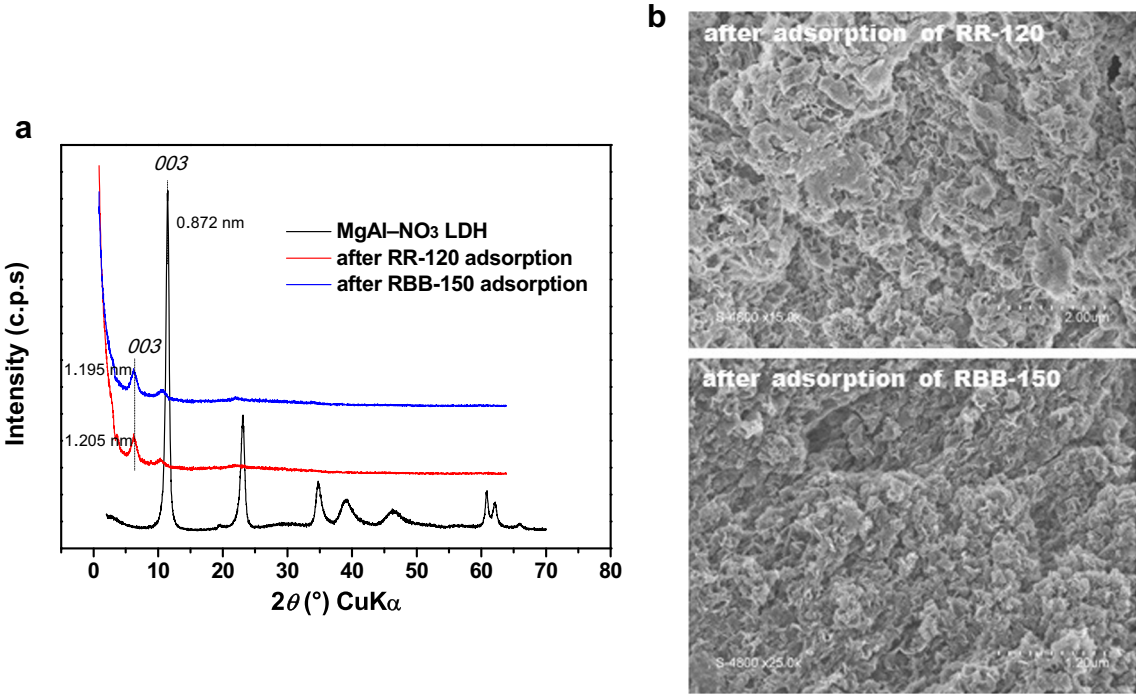

Fig. 11 PXRD patterns (**a**) and SEM images (**b**) of resulting samples after adsorption of RR-120 and RBB-150 onto MgAl-NO_3 LDH; C_0 = 500 mg/L

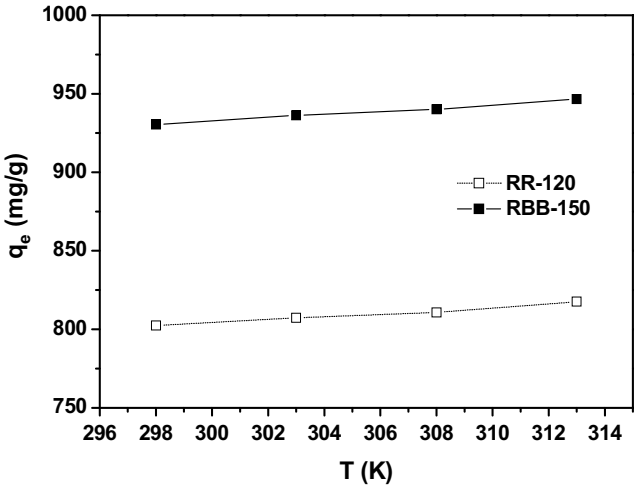

Fig. 12 Effect of temperature on the adsorption capacity of RR-120 and RBB-150 by MgAl-NO_3 LDH; $C_0 = 500$ mg/L, pH = 5, contact time of 120 min, adsorbent dosage of 50 mg

adsorption. After adsorption of RR-120 and RBB-150, the intensity of reflection peaks decrease dramatically; however, the *003* refection peaks shift to the right side and the basal spacing value d_{003} considerably increases to be 1.195 nm for RR-120 and 1.205 nm for RBB-150. This may indicate the partial exchange of nitrate anions from the internal space by dyes molecules. Thus, the adsorption process of RR-120 and RBB-150 involves two steps aimed at first the diffusion of dye molecules from liquid phase to the external surface of adsorbent via electrostatic forces and then from the external surface to the internal space of the adsorbent, indicating presumably that some dye molecules are intercalated probably in horizontally arrangement into the interlayer of LDH by mix effect including chemisorption and physisorption. Moreover, the presence of dye molecules on the surface of LDH (Fig. 11b) produced a change on the superficial interaction between particles that influences the crystallinity, the reorientation of the surface crystallites, and the aggregation between them.

Adsorption thermodynamics: effect of temperature

The variation of the adsorption capacity with temperature reflects on the feasibility of the adsorption. The obtained data in Fig. 12 shows that increase of temperature had improved the adsorption efficiency of RR-120 and RBB-150, indicating the endothermic nature of dye adsorption. The results demonstrate that with the higher temperature (that is higher kinetic energy), dye molecules are very mobile, which will facilitate their interaction with the active sites of the LDH adsorbent and overcome the bonding strength restricting the competiveness between them. The adsorption of 500-mg/L RR-120 or RBB-150 carried out at 25, 30, 35, and 40 °C had resulted in a gradually increase from 802.3 to 817.6 mg/g for RR-120 and from 930.4 to 946.6 mg/g for RBB-150.

By plotting ln $(\frac{q_t}{C_t})$ vs. $1/T$ Eq. (10), the thermodynamic parameters, such as change in standard free energy ($\Delta G°$), enthalpy ($\Delta H°$), and entropy ($\Delta S°$), Eq. (11) were evaluated and reported in Table 5.

$$\ln\left(\frac{Q_t}{C_t}\right) = \left(\frac{\Delta S^\circ}{2.303R}\right) - \left(\frac{\Delta H^\circ}{2.303RT}\right) \quad (10)$$

$$\Delta G^\circ = \Delta H^\circ - T\Delta S^\circ \quad (11)$$

where T is the temperature in Kelvin, and R is the gas constant (8.314 $Jmol^{-1}\ K^{-1}$).

Positive values of enthalpy ($\Delta H°$) confirms that the adsorption process of RR-120 and RBB-150 using MgAl-NO_3 LDH adsorbent is endothermic in nature, while the positive values of entropy ($\Delta S°$) suggest an increase in the randomness at the solid-solution interface. The negative values of free energy ($\Delta G°$) indicate that the adsorption of dyes onto the LDH was spontaneous; more negative the value, more energetically favorable the adsorption. In addition, the $\Delta G°$ values were in the range of (− 20–0 kJ/mol), suggesting a plausible physical adsorption for RR-120 and RBB-150, which is consistent with the previous results obtained by PXRD and SEM analyses after adsorption.

Effect of competitive inorganic anions

As interlayer inorganic anions are expected to interfere in the adsorption process of dye molecules, therefore, the adsorption experiments were carried out in the presence of various competing anions and the results are summarized in Fig. 13. The foreign inorganic anions investigated in this study were nitrate (NO_3^-), chloride (Cl^-), carbonate (CO_3^{2-}), and sulfate (SO_4^{2-}). The uptake study was done by taking each anion along with desired dye in different concentrations ratios (1/4, 1/2, 1/1, 3/2, and 2/1). The results (Fig. 13) showed in the first instance that as the concentration ratios of competitive anions

Table 5 Thermodynamic parameters for the adsorption of RR-120 and RBB-150 on MgAl-NO_3 LDH at several temperatures

Adsorbent	Dye	$\Delta H°$ (kJ/mol)	$\Delta S°$ ($J\ mol^{-1}\ K^{-1}$)	$\Delta G°$ (kJ/mol)			
				298 K	303 K	308 K	313 K
MgAl-NO_3 LDH	RR-120	2.15	16.24	− 2.68	− 2.77	− 2.85	− 2.93
	RBB-150	1.93	18.39	− 3.55	− 3.64	− 3.73	− 3.82

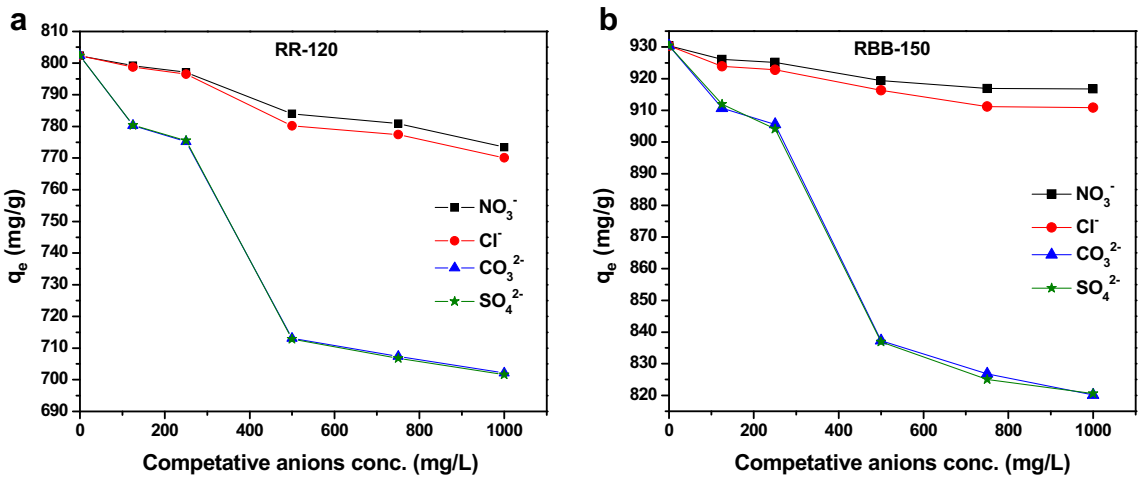

Fig. 13 Effect of interfering inorganic anion on the adsorption of **a** RR-120 and **b** RBB-150 by MgAl-NO_3 LDH; C_0 = 500 mg/L, pH = 5, contact time of 120 min, adsorbent dosage of 50 mg

to dye molecules were increased, adsorption capacity of LDH for RR-120 and RBB-150 was reduced. In addition, the presence of carbonate and sulfate anions influenced strongly on the uptake ability of dye molecules, while the other anions nitrate and chloride did not greatly influence on the uptake (Fig. 13). Thus, it is evident that the divalent anions have an intense interfering effect compared to monovalent anions in the following order: $CO_3^{2-} \approx SO_4^{2-} > Cl^- > NO_3^-$. This agree well with the LDH/anion affinity order proposed by Miyata (1983), which assumes that the LDH materials have more affinity toward anions with higher charge density.

Competition adsorption-desorption

To investigate whether the presence of RR-120 and RBB-150 dyes simultaneously in competitive system influences the removal efficiency of the LDH adsorbent, the adsorption efficiencies of each one in the 1:1 ratio of binary mixture were analyzed. Figure 14 shows the dye removal percentage of RR-120 and RBB-150 in the competitive experiment. Non-competitive trial data in single solution were used in the comparison. The results coincide with that previously found in single solution in which the adsorption rate of RBB-150 is always greater than of the RR-120. However, contrary to what was expected, the retention of dyes is slightly decreased in the mixture. Percentage removal of RR-120 was 74% (less of 6% than that of single solution) and that of RBB-150 is around 82% (less of 11% than that of single solution). A plausible explanation for the efficient dye uptake even though in binary solution is the exfoliation of the LDH layers, which increases the active sites of the adsorbent. PXRD pattern (Fig. 15) of the sample collected after adsorption in binary solution supports this hypothesis, in which a strong decrease of diffraction line intensities is observed. Their enlargement is thought by a greater disorder of the structure with a turbostratic effect. On the other hand, the amount percentages of the dyes released after desorption experiments were found to be at 8% for RR-120 and 20% for RBB-150 in single solution, and being a little bit higher

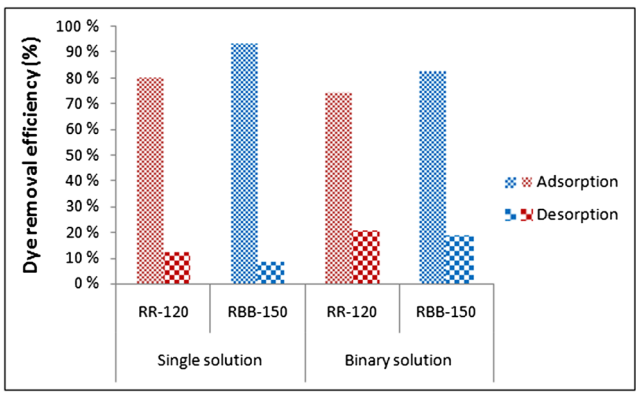

Fig. 14 Removal efficiency of RR-120 and RBB-150 in single and 1:1 binary ratio solutions; C_0 = 500 mg/L

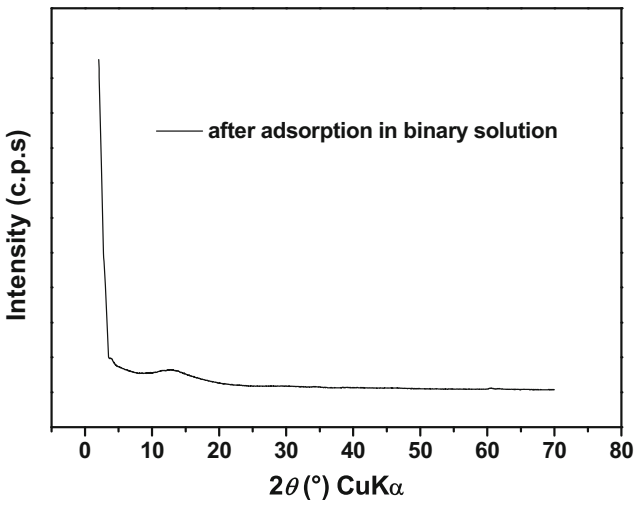

Fig. 15 PXRD pattern of collected sample after adsorption in binary solution

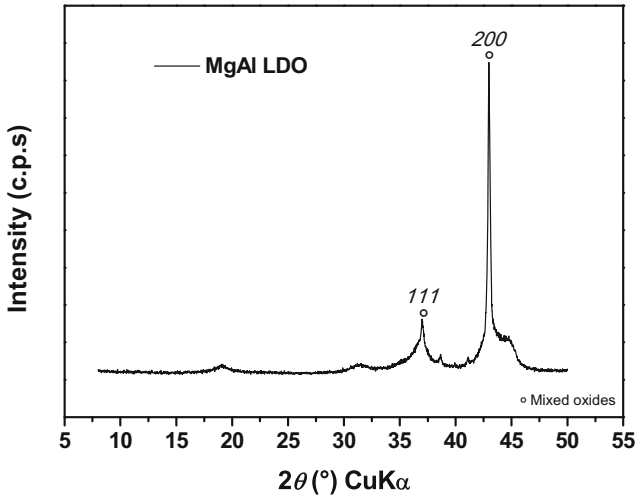

Fig. 16 Removal efficiency of RR-120 and RBB-150 after 5 cycles of adsorption-calcination-rehydration of the LDH adsorbent; C0 = 500 mg/L

in binary solution, nearly 20%, which indicates a strong affinity adsorbate/adsorbent, thereby hinders the desorption on the LDH.

Reusability cycling

The potential economical and environmental feasibility of applying the adsorbent LDH in recycling operation after adsorption experiments was investigated. Typically, the samples collected after adsorption of RR-120 and RBB-150 have undergone heat treatment at 500 °C for 4 h in order to decompose these dyes, due to their low removal by desorption processes (Crepaldi et al. 2002; Abdellaoui et al. 2017). The calcined product consisting of magnesium-aluminum-layered double oxide MgAl LDO (Fig. 16) was then rehydrated/reused to adsorb RR-120 and RBB-150 following the same adsorption experiment conditions. Figure 17 showed the reusability study of RR-120 and RBB-150 for 5 consecutive cycles (adsorption/calcination). The data showed that MgAl-NO_3 LDH exhibits a good stability after 5 cycles; the removal efficiency decreased gradually from 80 to 69% in single solution and from 74 to 60% in binary solution for RR-120 and from 93 to 80% in single solution and from 82 to 70% in binary solution for RBB-150. This decrease in the

Fig. 17 PXRD pattern of MgAl LDO

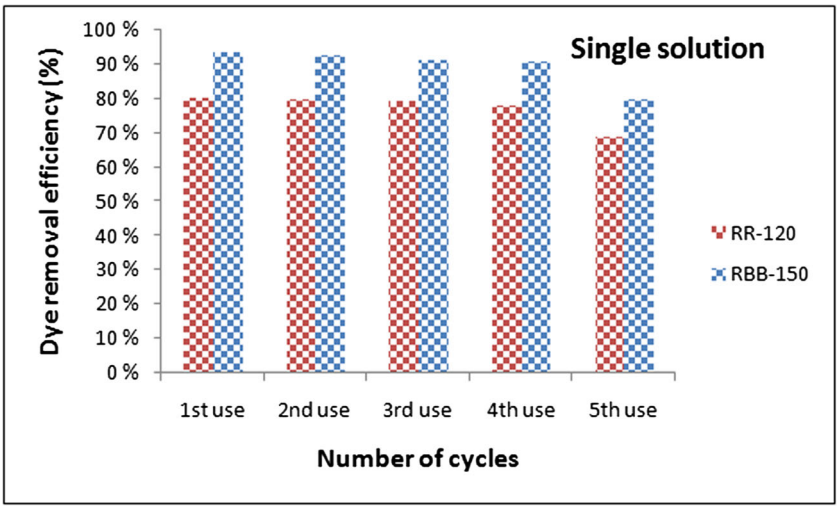

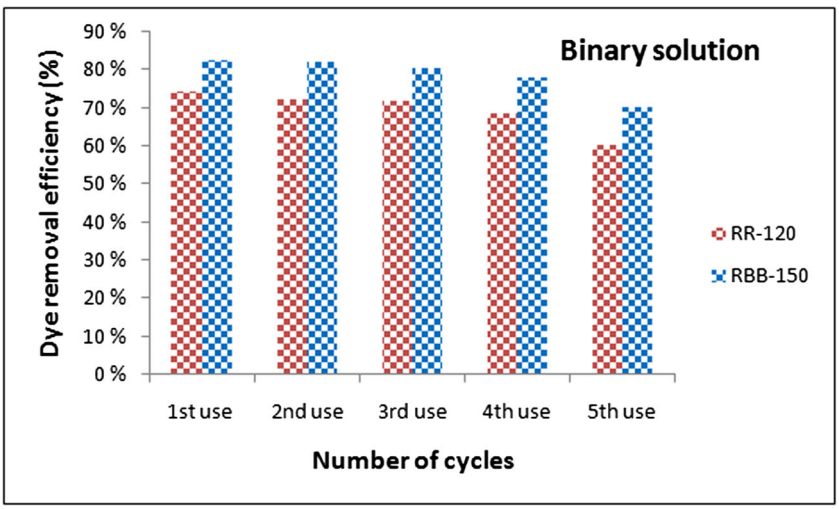

Table 6 Comparative studies of maximum adsorption capacity of various solid adsorbents involved in removal of RR-120 and RBB-150

Adsorbent	Initial conc. (mg/L)	RR-120 (mg/g)	RBB-150 (mg/g)	Reference
Cetylpyridinium-bentonite	1.4×10^{-4} mol L^{-1}	81.97	–	Tabak et al. 2010
Pumice	200	0.32	–	Hossein and Behzad 2012
Single-walled carbon nanotubes	200	1114.0	–	Bazrafshan et al. 2013
Natural clay (from Fouchana, Tunisia)	30	5.65	–	Abidi et al. 2014
Organophilic clay (with HDTMA)	80	22.8	–	Abidi et al. 2014
Carbon composite	300	95.76	–	Dos Santos et al. 2014
Natural clay (from Nabeul, Tunisia)	150	11.76	14.76	Naghmouchi and Nahdi 2015
Modified clay (with DMSO)	200	26.9	30.12	Naghmouchi and Nahdi 2016
MgAl-NO_3 LDH	500	800.0	910.0	Current work

removal ability can be related to the effect of specific surface area, which decreased after the fifth regeneration cycle to be 142 m^2/g. Such results is consistent with findings reported in literature and can be mainly explained by the progressive loss of crystallinity as well as the possibly interference of certain amount of decomposed dye compounds with the mixed metal oxides after thermal regeneration, which affecting the structural reconstruction of the calcined material (Zhu et al. 2005; Abdellaoui et al. 2017; Bessaha et al. 2017).

Comparative studies

The current removal capacity of the MgAl-NO_3 LDH adsorbent for RR-120 and RBB-150 was compared with some other obtained adsorption capacity of various adsorbents recently reported in literature (Table 6). Table 6 shows that the adsorption capacity of LDH for RR-120 and RBB-150 dyes is largely higher than that of the majority of the other adsorbent considered in literature, only the single-walled carbon nanotube (CNT) which has a relatively good adsorption capacity in comparison with our research work. CNTs are known as one of the first major adsorbents of a number of different organic pollutants due to their large specific surface area, high degree of surface reactivity, and large micropore volume (Ong et al. 2010; Tan et al. 2012). However, such impurities (amorphous carbon, fullerene, metal particles used for catalyst, etc.) in the as-prepared samples may have a detrimental effect on the utility and reliability of CNT as an adsorbents (Itkis et al. 2003; Wang and Pumera 2014) and need to be removed to ensure safely use in environmental applications. Although the CNT could generate fine particle that may contribute to environmental pollution, continuous production of CNT in large quantities is still far from being overcome. For these reasons, LDH may have advantageous potential as a green-adsorbent in wastewater treatment with low-cost and easy synthesis at large scale as well as future clean and sustainable material with no by-product after use.

Conclusions

In summary, removal of RR-120 and RBB-150 anionic textile dyes was investigated on MgAl-NO_3 LDH nanoparticles prepared by chemical co-precipitation method at constant pH value. PXRD, FTIR, SEM, TEM, and BET were carried out to investigate the physico-chemical features of the adsorbent. Although the lamellar structure, LDH showed a high surface area of 159 m^2/g and high exchange capacity of 360 mEq/100 g. The adsorption performance of LDH adsorbent was evaluated by investigating the influence of such adsorption conditions as initial pH value, contact time adsorbent dye, dye concentration, temperature, and competing interlayer anion. The synthesized material was characterized by a good adsorption capacity for both dyes. The adsorption was strongly pH-dependent; lower pH was more favorable for the removal of the anionic dyes. According to the equilibrium experiment, the maximum adsorption capacity has attained 800 mg/g for RR-120 and 910 mg/g for RBB-150 within 120 min of contact time at pH 5. The adsorption kinetic data fitted well to a pseudo-second-order as seen from the higher determination coefficient, and the adsorption equilibrium data reveal that the adsorption mechanism obeys Langmuir isotherm model, thus suggesting a physico-chemical adsorption mainly done in monolayer coverage. The thermodynamic parameters were calculated and showed that the adsorption was endothermic and spontaneous in nature. The single-point batch experiments demonstrated that nitrate interlayer anions have a minor influence on the removal of both dyes by MgAl-NO_3 LDH.

Furthermore, this work highlighted the competitive adsorption/desorption behavior of dye molecules at the interface of LDH nanoparticles, which is helpful to gain a deeper understanding of their interaction and immobilization in multi-dye contaminated water. And finally, reusability characteristics of spent adsorbent and its reconstructed form were studied and revealed the feasibility of recycling operation after 5 cycles of adsorption and thermal regeneration. Nevertheless, these results showed that MgAl-NO_3 LDH is particularly

promising candidate for the efficiency removal of RR-120 and RBB-150 dyes from wastewater.

Acknowledgments The authors would like to thank Dr. Martiane Cabié from "Centre Pluridisciplinaire de Microscopie Electronique et de Microanalyse (CP2M), Aix Marseille University, 13013 Marseille, France," for her assistance with microscopy analysis. Also, a huge thank you to the diffractometry and textural analysis services of "Institut Européen des Membranes (IEM), Montpellier University, 34090 Montpellier, France."

Compliance with ethical standards

Conflict of interest The authors declare that there is no conflict of interest.

References

Abdellaoui K, Pavlovic I, Bouhent M, Benhamouc A, Barriga C (2017) A comparative study of the amaranth azo dye adsorption/desorptionfrom aqueous solutions by layered double hydroxides. Appl Clay Sci 143:142–150

Abidi N, Duplay J, Ayari F, Gangloff S, Trabelsi-Ayadi M (2014) Adsorption of anionic dye on natural and organophilic clays: effect of textile dyeing additives. Desalin Water Treat:1–16

Ai L, Zhang C, Liao F, Wang Y, Li M, Meng L, Jiang J (2011) Removal of methylene blue from aqueous solution with magnetite loaded multi-wall carbon nanotube: kinetic, isotherm and mechanism analysis. J Hazard Mater 198:282–290

Aguiar JE, Bezerra BTC, Siqueira ACA, Barrera D, Sapag K, Azevedo DCS, Lucena SMP, Silva Jr IJ (2014) Improvement in the adsorption of anionic and cationic dyes from aqueous solutions: a comparative study using aluminum pillared clays and activated carbon. Sep Sci Technol 49:741–751

Anbia M, Hariri SA (2010) Removal of methylene blue from aqueous solution using nanoporous SBA-3. Desalination 261(1–2):61–66

Bazrafshan E, Mostafapour FK, Hosseini AR, Khorshid AR, Mahvi AH (2013) Decolorisation of Reactive Red 120 dye by using single-walled carbon nanotubes in aqueous solutions. J Chem:1–8

Bessaha H, Bouraada M, Deménorval LC (2017) Removal of indigo carmine and green bezanyl-F2B from water using calcined and uncalcined Zn/Al þ Fe layered double hydroxide. J Water Reuse Desal 07(2):152–161

Carretero MI (2002) Clay minerals and their beneficial effects upon human health. A review. Appl Clay Sci 21:155–163

Chitrakar R, Tezuka S, Sonoda A, Sakane K, Hirotsu T (2008) A new method for synthesis of Mg-Al, Mg-Fe, and Zn-Al layered double hydroxides and their uptake properties of bromide ion. Ind Eng Chem Res 47:4905–4908

Crepaldi EL, Tronto J, Cardoso LP, Valim JB (2002) Sorption of terephthalate anions by calcined and uncalcined hydrotalcite-like compounds. Colloids Surf A Physicochem Eng Asp 211:103–114

Darsana A, Chandrasehar G, Deepa V, Gowthami Y, Chitrikha T, Ayyappan S, Goparaju A (2015) Acute toxicity assessment of Reactive Red 120 to certain aquatic organisms. Bull Environ Contam Toxicol 95:582–587. https://doi.org/10.1007/s00128-015-1636-z

Delhoyo C (2007) Layered double hydroxides and human health: an overview. Appl Clay Sci 36:103–121

Djebbi MA, Braiek M, Namour P, Ben Haj Amara A, Jaffrezic-Renault N (2016) Layered double hydroxide materials coated carbon electrode: new challenge to future electrochemical power devices. Appl Surf Sci 386:352–363

Dos Santos AB, Cervantes FJ, Lier JB (2007) Review paper on current technologies for decolourisation of textile wastewaters: perspectives or anaerobic biotechnology. Bioresour Technol 98:2369–2385

Dos Santos DC, Adebayo MA, De Fátima Pinheiro Pereira S, Prola LDT, Cataluña R, Lima EC, Saucier C, Gally CR, Machado FM (2014) New carbon composite adsorbents for the removal of textile dyes from aqueous solutions: kinetic, equilibrium, and thermodynamic studies. Korean J Chem Eng 31(8):1470–1479

El Hassani K, Beakoua BH, Kalnina D, Oukani E, Anouar A (2017) Effect of morphological properties of layered double hydroxides on adsorption of azo dye Methyl Orange: a comparative study. Appl Clay Sci 140:124–131

Errais E, Duplay J, Elhabiri M, Khodja M, Ocampo R, Baltenweck-Guyot R, Darragi F (2012) Anionic RR120 dye adsorption onto raw clay: surface properties and adsorption mechanism. Colloids Surf A Physicochem Eng Asp 403:69–78

Evans DG, Duan X (2006) Preparation of layered double hydroxides and their applications as additives in polymers, as precursors to magnetic materials and in biology and medicine. Chem Commun 42:485–496

Evans DG, Slade RCT (2006) Structural aspects of layered double hydroxides, 119. Structural and bonding. Springer, Berlin, pp 1–87

Feng JT, Ma X, He Y, Evans DG, Li DQ (2012) Synthesis of hydrotalcite-supported shape-controlled Pd nanoparticles by a precipitation-reduction method. Appl Catal A 413–414:10–20

Forano C (2004) Environmental remediation involving layered double hydroxides in clay surfaces. In: Wypych F, Satyanarayana KG (eds) Fundamentals and applications. Elsevier Academic Press, New York, pp 425–458

Giles CH, Smith D, Hintson A (1974) General treatment and classification of solute adsorption-isotherm 1. Theoretical. J Colloid Interface Sci 47:755–765

Gu Z, Atherton JJ, Xu ZP (2015) Hierarchical layered double hydroxide nanocomposites: structure, synthesis and applications. Chem Commun 51:3024–3036

Ho YS, McKay G (1999) Pseudo-second order model for sorption processes. Process Biochem 34:451–465

Hossein MA, Behzad H (2012) Removal of Reactive Red 120 and Direct Red 81 dyes from aqueous solutions by Pumice. Res J Chem Environ 16(1):62–68

Itkis ME, Perea DE, Niyogi S, Rickard SM, Hamon MA, Hu H, Zhao B, Haddon RC (2003) Purity evaluation of as-prepared single-walled carbon nanotube soot by use of solution-phase near-IR spectroscopy. Nano Lett 3(3):309–314

Lagergren S (1898) Kungliga Svenska Vetenskapsakademiens, Handlingar. Band 24:1–39

Langmuir I (1918) The adsorption of gases on plane surfaces of glass, mica and platinum. J Am Chem Soc 40:1361–1403

Liang X, Zang Y, Xu Y, Tan X, Hou W, Wang L, Sun Y (2013) Sorption of metal cations on layered double hydroxides. Colloids Surf A Physicochem Eng Asp 433:122–131

Mahjoubi FZ, Khalidib A, Abdennouria M, Barkaa N (2017) Zn–Al layered double hydroxides intercalated with carbonate, nitrate, chloride and sulphate ions: synthesis, characterisation and dye removal properties. J Taibah Univ Sci 11:90–100

McMullan G, Meehan C, Conneely A, Kirby N, Robinson T, Nigam P, Banat IM, Marchant R, Smyth WF (2001) Microbial decolourisation and degradation of textile dyes. Appl Microbiol Biotechnol 56:81–87

Miyata S (1983) Anion-exchange properties of hydrotalcite-like compounds. Clay Clay Miner 31:305–311

Naghmouchi N, Nahdi K (2015) Adsorption of textile dyes on raw Tunisian clay: equilibrium, kinetics and thermodynamics. J Adv Chem 11(6):3685–3697

Naghmouchi N, Nahdi K (2016) Equilibrium, kinetics and thermodynamics studies of textile dyes adsorption on modified Tunisian clay. Mediterranean J Chem 5(2):414–422

Ong YT, Ahmad AL, Zein SHS, Tan SH (2010) A review on carbon nanotubes in an environmental protection and green engineering perspective. Braz J Chem Eng 27(02):227–242

Özcan AS, Özcan A (2004) Adsorption of acid dyes from aqueous solutions onto acid-activated bentonite. J Colloid Interface Sci 276:39–46

Pereira WS, Freire RS (2005) Ferro zero: Uma nova abordagem para o tratamento de águas contaminadas com compostos orgânicos poluentes. Quim Nova 28:130–136

Perez-Ramírez J, Mul G, Kapteijn F, Moulijn JA (2001) In situ investigation of the thermal decomposition of Co–Al hydrotalcite in different atmospheres. J Mater Chem 11:821–830

Rives V (2001) Layered double hydroxides: present and future. Nova Science Publishers, Inc, New York

Robinson T, Chandran B, Nigam P (2002) Removal of dyes from a synthetic assay and different water extraction procedures. Chemosphere 54:1589–1597

Rojas R (2012) Layered double hydroxides applications as sorbents for environmental remediation. In: Calixto A, Analiz D (eds) Hydroxides: synthesis, types and applications. Nova Science Publishers, Inc., New York, pp 39–71 (Chapter 2)

Santhosh C, Velmurugan V, Jacob G, Jeong SK, Grace AN, Bhatnagar A (2016) Role of nanomaterials in water treatment applications: a review. Chem Eng J 306:1116–1137

Santos RMM, Tronto J, Brioisc V, Santilli CV (2017) Thermal decomposition and recovery properties of ZnAl–CO_3 layered double hydroxide for anionic dye adsorption: insight into the aggregative nucleation and growth mechanism of the LDH memory effect. J Mater Chem A 5:9998–10009

Singh K, Arora S (2011) Removal of synthetic textile dyes from wastewaters: a critical review on present treatment technologies. Crit Rev Environ Sci Technol 41:807–878

Tabak A, Baltas N, Afsin B, Emirik M, Caglar B, Eren E (2010) Adsorption of Reactive Red 120 from aqueous solutions by cetylpyridinium-bentonite. J Chem Technol Biotechnol 85:1199–1207

Tan CW, Tan KH, Ong YT, Mohamed AR, Zein SHS, Tan SH (2012) Energy and environmental applications of carbon nanotubes. Environ Chem Lett 10:265–273

Wang L, Pumera M (2014) Residual metallic impurities within carbon nanotubes play a dominant role in supposedly "metal-free" oxygen reduction reactions. Chem Commun 50(84)

Weber WJ, Morris JC (1963) Kinetics of adsorption on carbon solution. J Sanit Eng Div ASCE 89:31–59

Zhang B, Dong Z, Sun D, Wu T, Li Y (2017) Enhanced adsorption capacity of dyes by surfactant-modified layered double hydroxides from aqueous solution. J Ind Eng Chem 49:208–218

Zhu M-X, Li Y-P, Xie M, Xin H-Z (2005) Sorption of an anionic dye by uncalcined and calcined layered double hydroxides: a case study. J Hazard Mater 120:163–171

Zubair M, Daud M, McKayd G, Shehzad F, Al-Harthi MA (2017) Recent progress in layered double hydroxides (LDH)-containing hybrids as adsorbents for water remediation. Appl Clay Sci 143:279–292